Sensors and Actuators B 258 (2018) 408–414

Contents lists available at ScienceDirect

Sensors and Actuators B: Chemical

journal homepage: www.elsevier.com/locate/snb

Development of a selective fluorescence nanosensor based on molecularly imprinted-quantum dot optosensing materials for saxitoxin detection in shellfish samples

Aili Sun[a,1], Jiye Chai[a,1], Tingting Xiao[a], Xizhi Shi[a,c,*], Xunjia Li[a], Qiaoling Zhao[b], Dexiang Li[a], Jiong Chen[a,c]

[a] School of Marine Sciences, Ningbo University,818 Fenghua Road, Ningbo 315211, PR China
[b] Zhoushan Institute for Food and Drug Control, Zhoushan 316021, PR China
[c] Collaborative Innovation Center for Zhejiang Marine High-efficiency and Healthy Aquaculture, Ningbo 315211, PRChina, China

ARTICLE INFO

Article history:
Received 24 July 2017
Received in revised form
20 November 2017
Accepted 22 November 2017
Available online 23 November 2017

Keywords:
Quantum dot
Molecularly imprinted
Saxitoxin
Nanosensor

ABSTRACT

A new type of molecularly imprinted silica layers appended to quantum dots (MIP-QDs) for saxitoxin (STX) was fabricated through the surface grafting technique. The MIP-QDs were characterized by scanning electron microscopy (SEM), transmission electron microscopy (TEM), fourier transform infrared spectroscopy (FT-IR), and imprinting and selective fluorescence quenching properties in different solutions.

Results demonstrated that the synthesized MIP-QDs exhibited excellent selective fluorescence quenching to STX because of the complementary imprinted cavities on the surface of MIP-QDs. Furthermore, a fluorescence nanosensor based on MIP-QDs was fabricated for the selective detection of STX under optimal experimental conditions. A good linear relationship in the range of 20.0-100.0 μg/L with a correlation coefficient of 0.9988 was obtained. Excellent recoveries ranging from 89.4% to 102.4% with the RSD below 6.3% were obtained for the shellfish samples at three spiked levels of STX. The detection limit of STX in shellfish samples was 0.3 μg/kg. The results indicated that the developed fluorescence nanosensor was highly selective and sensitive enough to detect STX in shellfish samples.

1. Introduction

Paralytic shellfish toxins (PSTs), mainly including saxitoxin (STX) and its analogs, are marine toxins commonly produced by genera *Alexandrium, Gymnodinium,* and *Pyrodinium* [1,2]. Among PSTs, STX is the most common toxic PST with LD_{50} value of 10.0 μg/kg in mice [3,4], which can block the neuronal transmission between nerves and muscle cell membranes by binding to the voltage-gated Na^+ channel, resulting in subsequent disturbance of neuromuscular transmission and voluntary muscle paralysis [4–6]. Particularly, STX has a strong tolerance to high temperatures and acidic environments and can not be destroyed by common treatments [7–9].

Due to the accumulation in filter-feeding bivalves and fish, the STX shows detrimental effects on human health and shellfish industry. Therefore, many countries, such as the United States, Canada, and most countries in Europe, established the STX maximum level of 80.0 μg/100 g in fresh shellfish [10], and mouse bioassay method established by Sommer and Mayer in 1937 is accepted internationally as the standard method for the quantitative measurement of PSP in shellfish according to the Association of Analytical Communities (AOAC) [11]. However, this method shows low sensitivity and accuracy and is accompanied with cumbersome operation and cultivation of animals [12,13]. Now, high-performance liquid chromatography (HPLC) coupled with fluorescence or mass spectrometry (MS) is also adapted by AOAC because they are highly sensitive and accurate [14]. However, these instrumental analysis technologies require complex preprocesses, expensive cost and professional operators. Therefore, the rapid, low-cost, and low-sample consumption sensor method on the basis of fluorescence, electrochemistry, surface plasmon resonance, and enzyme-linked immunosorbent assays for STX detection are being developed and exhibited excellent sensitivity and accuracy [15–18]. Neverthe-

* Corresponding author at: School of marine sciences Ningbo University 818 Fenghua Road, Ningbo 315211 PR China.
E-mail address: shixizhi@nbu.edu.cn (X. Shi).
[1] These authors contributed equally to this work.

https://doi.org/10.1016/j.snb.2017.11.143
0925-4005/

less, the major drawback of these methods is the antibody usage as recognition element, which commonly requires sophisticated production processes, experimental animals, and special storage conditions for stability [19]. Molecular imprinting is an alternative approach in designing artificial antibodies that possesses specific molecular recognition properties similar or superior to biological antibodies. These artificial antibodies had successfully applied to biomimetic sensors as recognition elements [20,21].

Meanwhile, quantum dots (QDs), a semiconductor nanoparticle, have size-dependent optical and electronic properties, narrow emission spectra, broad absorption spectra, and exhibit high resistance to photobleaching and thus can potentially improve the signal response of sensor-based MIPs [22]. In particular, the MIPs functionalize the surfaces of QDs to realize high selective fluorescence sensing. At present, molecularly imprinted silica layers appended to quantum dots (MIP-QDs) are fabricated and successfully used as recognition and response probes of sensors in detecting analytes, such as metronidazole, pesticides, toxins, and endocrine disruptors [23–26]. These sensors show special selective recognition and sensitive fluorescence signal response to template molecules. However, to the best of our knowledge, an fluorescence nanosensor based on MIP-QDs for STX detection in shellfish samples is not yet reported. The present study first fabricated MIP-QDs through surface imprinting technique and successfully constructed an fluorescence nanosensor to selectively detect STX.

2. Experimental

2.1. Materials and chemicals

STX, okadaic acid (OA), gonyautoxin (GTX), anatoxin-a (ATX), and neosaxitoxin (NEO) were purchased from the National Research Council (Halifax, NS, Canada). Tetraethyl orthosilicate (TEOS), 3-aminopropyl triethoxysilane (APTES) and triton X-100 were obtained from Sigma-Aldrich (Steinheim, Germany). QDs (CdS/CdSe/ZnS) with excitation and emission wavelengths of 270 and 618 nm, respectively, were purchased from Bedajubang Science and Technology Co., Ltd. (Beijing, China). Ammonia (25.0%-28.0%, v/v), acetone, and cyclohexane were obtained from Sinopharm Chemical Reagent Co., Ltd. (Shanghai, China). High-purity water was obtained from laboratory ultrapure water device (Ulupure, Sichuan, China). All other reagents used in experiments were of analytical grade.

2.2. Synthesis of MIP-QDs

Modified reverse micro-emulsion was performed to prepare MIP-QDs [27]. Briefly, 1.8 mL of TritonX-100 was added to 7.5 mL of cyclohexane, and the resulting mixture was magnetically stirred for 15 min. Subsequently, 400.0 μL of QDs (500.0 μg), 50.0 μL of TEOS, and 100.0 μL of ammonia (25.0%-28.0%, v/v) were sequentially added. After stirring for 2 h, 15.6 μL of STX (1.0 mg/mL, dissolved in methanol) and 22.8 μL of APTES were added to methanol (0.2 mL) and reacted with the above mixture for 12 h at room temperature. Acetone (10.0 mL) was then used to break the micro-emulsion, and the mixture was centrifuged at 8.0×10^3 g for 10 min. The pellets were washed with 6.0 mL of water to remove the unreacted TEOS and APTES. Finally, the template was extracted with ethanol/acetonitrile (8:2, v/v) until no template was detected by LC–MS. Nonimprinted silica layers appended to quantum dots (NIP-QDs) were simultaneously synthesized without the template.

2.3. Instruments and measurements

Fluorescence detection was performed by F-4600 spectrophotometer (Hitachi, Japan) equipped with a quartz cell (1 cm × 1 cm). Fourier transform infrared spectroscopic (FT-IR) measurements were conducted on a Nicolet 6700 Fourier infrared spectrometer (Thermo, USA). Scanning electron microscopy (SEM) and transmission electron microscopy (TEM) images were obtained using Model S-4800 electron scanning microscope (Hitachi, Japan) and Model H-7650 transmission electron microscope (Hitachi, Japan), respectively. The surface area and pore size distribution of MIP-QDs and NIP-QDs were analyzed using a micromeritics ASAP 2020 analyzer instrument (Norcross, GA, USA)

2.4. Fluorescence measurement

For the detection of STX, the conditions of fluorescence measurement were as follows: the slit widths of the excitation and emission were 5.0 and 10.0 nm, the excitation wavelength was set to 270 nm, and the range of the emission wavelength was set to 560–700 nm with a photomultiplier tube voltage of 700 eV. MIP-QDs were dispersed into an appropriate solution with the final concentration of 15.0 mg/mL. An appropriate volume of STX standard solution was added to the cell. The fluorescence intensity at the maximum emission wavelength of 618 nm was measured. The experiments were conducted in triplicate.

2.5. Selectivity analysis of MIP-QDs

Under optimal conditions, the selectivity of the MIP-QDs was investigated by comparing the fluorescence quenching of STX and its analogs including ATX-a, GTX, NEO, and OA. Fluorescence quenching was calculated according to the Stern-Volmer equation: $F_0/F = 1 + Ksv[Q]$ [27], where F_0 and F are the fluorescent intensities of MIP-QDs in the absence and presence of various STX concentrations, respectively, *Ksv* is the Stern-Volmer quenching constant of STX, and [Q] is the STX concentration. The imprinting factor (IF) was defined as the ratio between the *Ksv* values of MIP-QDs and NIP-QDs and used to evaluate the selectivity of the MIP-QDs [27].

2.6. Sample preparation

Shellfish samples were obtained from a local market and stored frozen until analysis. Exactly 2.0 g homogenized shellfish samples were weighed in 15.0 mL polypropylene tubes. Afterwards, 4.0 mL of acetonitrile/water/formic acid (80:20:0.1, v/v/v) were added, ultrasonicated for 10 min, and then centrifuged at 4.5×10^3 g for 10 min. The supernatant was collected and frozen at −20 °C for 1 h. After quick filtration, the filtrate was dried at N_2 atmosphere, and the residues were resuspended in 1.0 mL of water with 0.1% formic acid. Subsequently, 50.0 mg of C_{18} and 50.0 mg of acidic alumina were added, immediately vortexed for 1.0 min and centrifuged at 4.5×10^3 g for 10 min. Finally, the supernatant was filtered through a 0.22 μm nylon filter for analysis.

3. Results and discussion

3.1. Preparation of MIP-QDs based on QDs

The strategy for the synthesis of MIP-QDs based on CdS/CdSe/ZnS QDs is illustrated in Fig. 1. The MIP-QDs were synthesized through reverse microemulsion. The imprinted silica layers were successfully fabricated onto the QDs surface via the hydrolysis and condensation reaction of TEOS and APTES, which provide the $-NH_2$ surface binding sites on the QD surface and effectively improve the fluorescence stability of the QDs by inhibiting photo-oxidation. The fluorescence was quenched after adding the template but was recovered when the template was extracted. In this study, the number of initial QDs was optimized by determining the fluorescence intensity due to the nimiety or

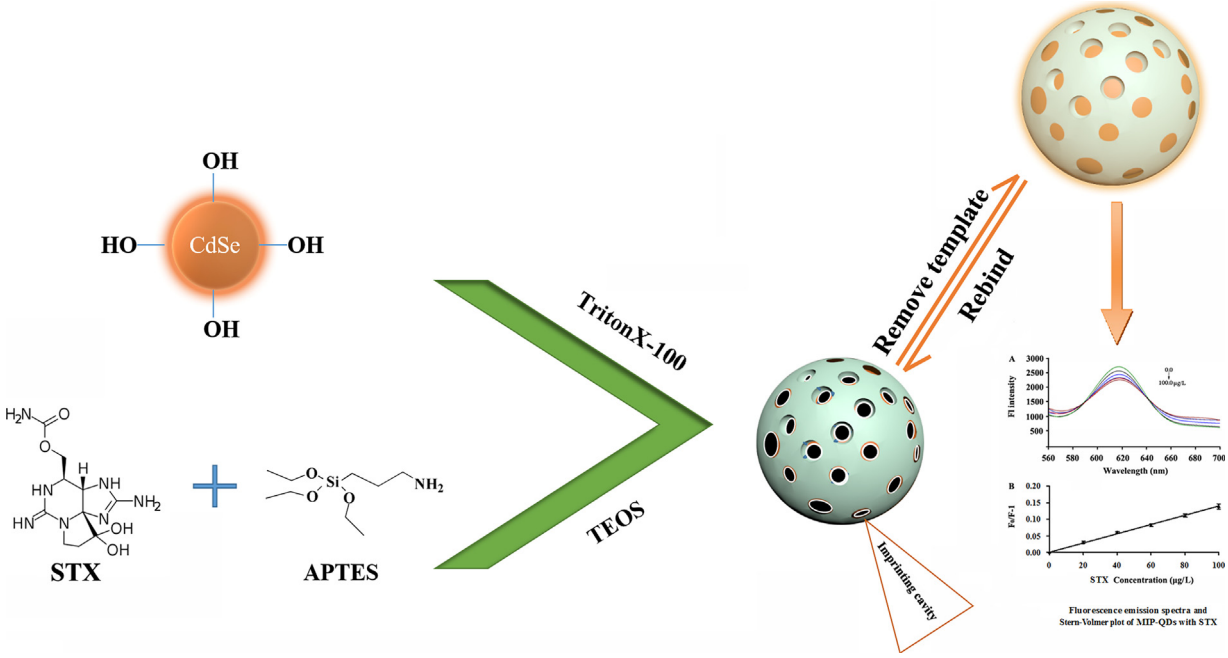

Fig. 1. Schematic diagram for the preparation of MIP-QDs and fluorescence nanosensor for STX detection.

lack of QDs, resulting in fluorescence quenching or weakening. As shown in Fig. 2, the fluorescence intensities of the MIP-QDs increased gradually and reached a maximum at 1.25 mg/mL at increasing amount of QDs. Subsequently, the fluorescence decreased when the amount of QDs increased. The reason may be the self-quenching phenomenon induced by excessive QDs coated onto the MIP-QDs [28]. Therefore, the 1.25 mg/mL QD concentration was selected for MIP-QD synthesis.

3.2. Characterization of MIP-QDs

The morphological structure and particle size of the fabricated MIP-QDs were analyzed by SEM and TEM. As shown in Fig. 3, MIP-QDs and NIP-QDs were spherical monodispersed with an average diameter of approximately 40 nm. MIP-QDs and NIP-QDs have no difference in their morphological structure. Nevertheless, MIP-QDs have larger external surface area (MIP-QDs, $130.4 \pm 1.3\ m^2/g$; NIP-QDs,$108.2\ m^2/g$) and total pore volume (MIP-QDs, $0.74 \pm 0.01\ m^3/g$; NIP-QDs,$0.57\ m^3/g$) than NIPs, indicating that the MIP-QDs can provide more specific recognition sites to the quencher than the NIPs.

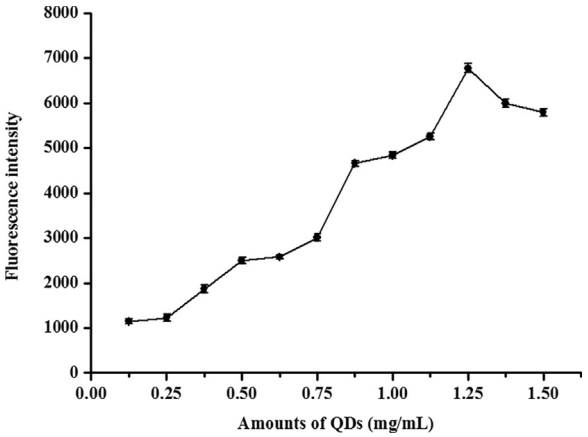

Fig. 2. Effect of QD concentrations on the fluorescence intensity of MIP-QDs, MIP-QD amount: 15.0 mg/L.

The FT-IR spectra of the MIP-QDs and NIP-QDs were characterized to check whether the MIPs were chemically coated onto the QDs and elucidate the fluorescence quenching mechanism. As illustrated in Fig. 4, the peak at 1047 cm^{-1} is the characteristic peak of the stretching vibration of Si—O—Si. The broad peak around 455 and 787 cm^{-1} is the Si—O stretching vibration peak. Peaks near the peak widths of 3427, 2937, and 1562 cm^{-1} are the C—H and N—H stretching vibration peaks. These bands suggested that the $-NH_2$ of APTES was grafted onto the surface of the QDs. Meanwhile, no significant difference was observed between the spectral patterns of the MIP-QDs and NIP-QDs, indicating that MIP-QDs and NIP-QDs have similar main components [29].

3.3. Optosensing of STX by MIP-QDs

The complementary imprinting cavities in size, shape, and position of the functional group to template onto the surface of MIP-QDs dominate the specific recognition and fluorescence quenching. Therefore, the optimal system of different ratios of H_2O to ethanol and pH was investigated to acquire the best fluorescence quenching response due to the swelling and shrinking effect of the imprinted sol-gel layers of MIP-QDs. Imprinting factor (IF) was defined as the ratio of the $K_{SV.MIP\text{-}QDs}$ and $K_{SV.NIP\text{-}QDs}$ and was used to evaluate the selective FL quenching of the MIP-QDs.

As shown in Fig. 5A, the largest IF (3.30) of the MIP-QDs was obtained in the ethanol solvent. However, an IF value of 2.94 in H_2O: ethanol solvent (30:70, v/v) was simultaneously obtained. These results confirmed that the MIP-QDs exhibited specific binding and fluorescence quenching to the template through the efficient imprinting effect as compared with NIP-QDs. Hydrogen bonds and hydrophobic interactions play important roles in the appropriate swelling of sol-gel imprinting cavities onto the surface of MIP-QDs. Given that STX is usually extracted using acidic aqueous solutions because of its hydrophilic structure, the H_2O: ethanol solvent (30:70, v/v) was selected for the subsequent experiments.

Owing to the alkaline nature of STX in an aqueous solution, the interaction between STX and MIP-QDs is expected to improve at an acidic condition. Especially, STX occurs mainly in ionic form and is stable in acidic conditions but not in basic condition because it

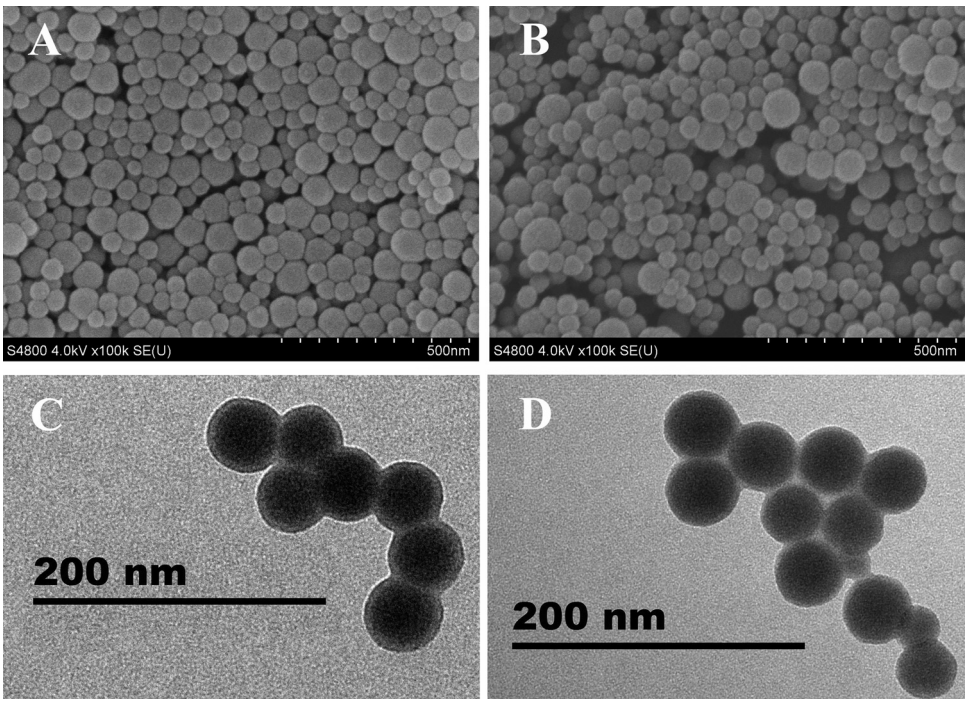

Fig. 3. SEM images of MIP-QDs (A) and NIP-QDs (B). TEM images of MIP-QDs (C) and NIP-QDs (D).

can be easily oxidized [30]. Therefore, the existing states of MIP-QDs surface groups were affected as well by the pH of the working solution. The effects of pH 3.0-9.0 on the selectivity of MIP-QDs and NIP-QDs to STX were investigated. As shown in Fig. 5B, the fluorescence signals and IF value increased at pH of 3.0–6.0 and then decreased at pH of 6.0–9.0. The strongest FL signals (Fig. 5C) of the MIP-QDs were observed at pH 6.0, and the best imprinting effect was simultaneously obtained at IF value of 3.21. Thus, pH of 6.0 was selected for further experiments.

Excessive MIP-QDs results in low sensitivity to STX, whereas an insufficient amount can cause a narrow linear range [31]. Therefore, MIP-QDs concentrations of 5.0-25.0 mg/L were selected to elucidate its effects on fluorescence quenching. As shown in Fig. 6, the fluorescence quenching (F_0-F) increased at increased amount of MIP-QDs (5.0–15.0 mg/L). Nevertheless, FL quenching was not increased when the MIP-QD amount was higher than 15.0 mg/Land the highest quenching efficiency was obtained at 15.0 mg/L. Therefore, the optimum value of 15.0 mg/L was applied throughout the work.

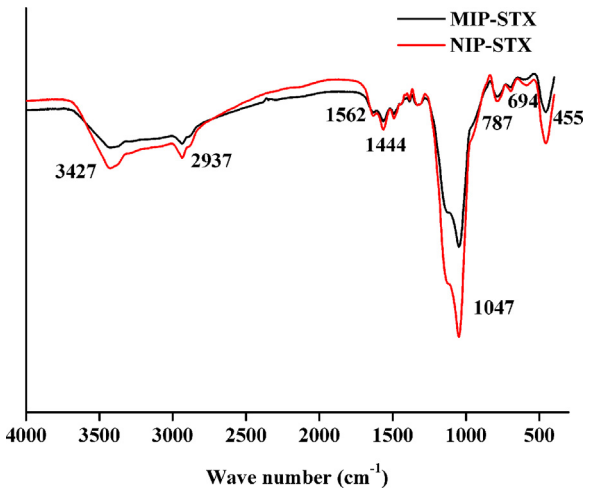

Fig. 4. FT-IR spectra of MIP-QDs and NIP-QDs.

The optimal response time of the fluorescence quenching for STX was further studied. After adding the STX, the FL intensity curve of MIP-QDs decreased within 6 min of reaction and then became flat. Therefore, 6 min detection time was selected for subsequent experiments.

3.4. Selectivity and interference study of MIP-QDs

When STX was removed, the imprinted sites remained on the surface of MIP-QDs. The mechanism of selective fluorescence quenching may be considered as the optical properties of QDs and differential chemical structures of the analogs [30]. Therefore, several kinds of STX structural analogs, including GTX, NEO, ATX, and OA, were applied to evaluate the selectivity of MIP-QDs. The fluorescence quenching and selectivity of the MIP-QDs on the quencher were evaluated. As shown in Fig. 7, the strongest fluorescence quenching (F_0-F) and the highest IF value of STX to MIP-QDs were obtained than those of its analogs, and IF values of its analogs were all lower than 1.0, whereas, the similar low levels fluorescence quenching capability of STX and its analogs to NIP-QDs were found, which indicated that the high specific fluorescence quenching response of MIP-QDs to STX were occurred and the imprinted cavities were absent on the surfaces of the NIP-QDs. The STX and its analogs GTX, NEO, and ATS have a similar chemical structure and tetrahydropurine backbone but different functional groups, suggesting that the imprinted cavities, which have complementary sites for STX, fabricated onto the QD surfaces played an important role in the selective fluorescence quenching of MIP-QDs. Furthermore, the effect of shellfish extract matrices on the fluorescence quenching performance of the MIP-QDs was studied. The fluorescence intensity and quenching of MIP-QDs in pure solvent were compared with those in the sample extractant. As shown in Fig. 8, negligible fluorescence quenching response (F_0-F) and quenching efficiency ((F_0-F)/F_0) was observed between the sample and pure solvent, indicating that no distinct interferences induced by the matrix effect were found.

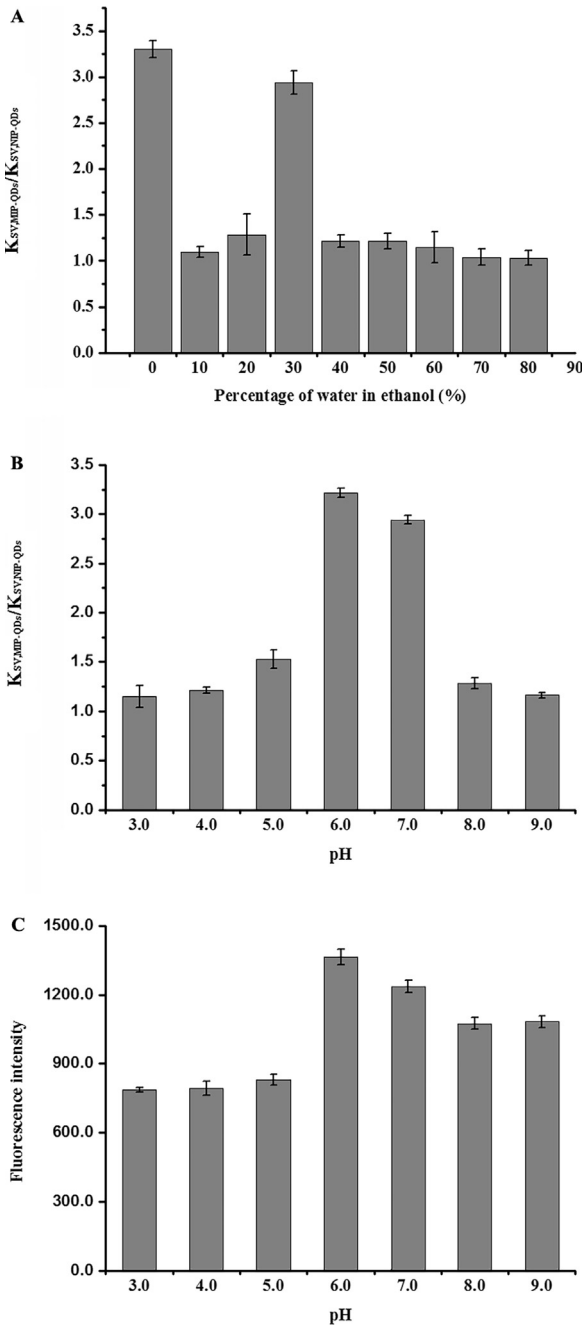

Fig. 5. Effect of different reaction solutions on the selectivity and fluorescence intensity of MIP-QDs. (A) Effect of ratio of H_2O to ethanol on MIP-QD selectivity; (B) Effect of pH on MIP-QD selectivity; (C) Effect of pH on fluorescence intensity of MIP-QDs.

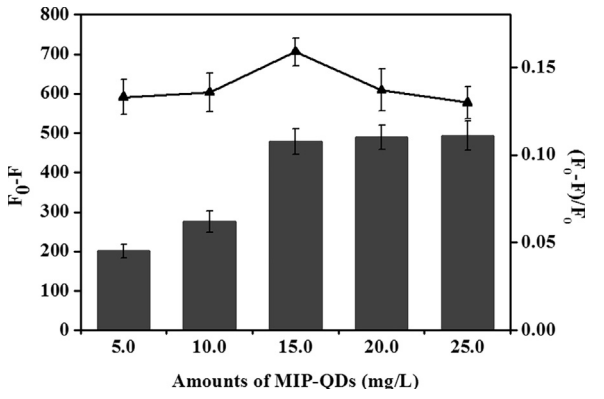

Fig. 6. Effect of MIP-QD amounts on fluorescence quenching (the bars) and quenching efficiency (the triangles). MIP-QDs, 15.0 mg/L; STX concentration, 60.0 μg/L.

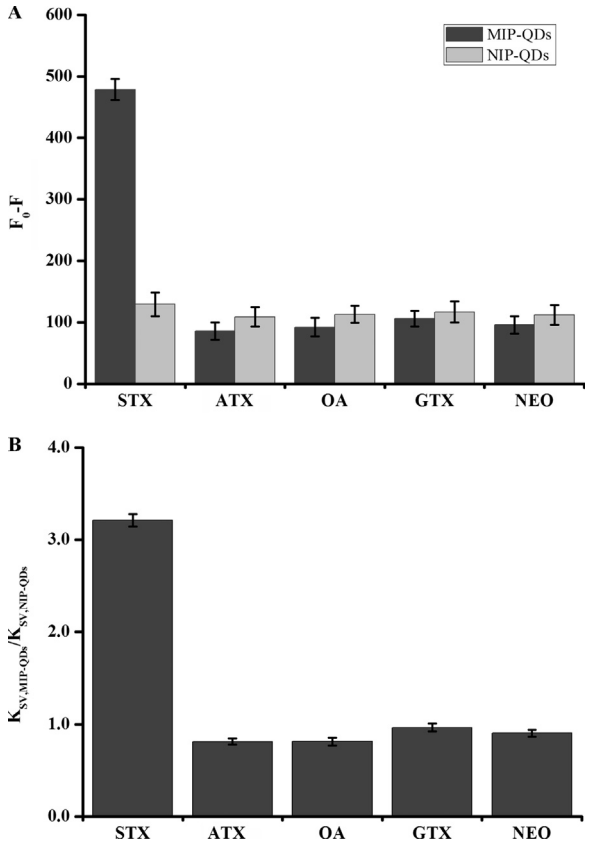

Fig. 7. Selectivity of MIP-QDs and NIP-QDs to STX, ATX, OA, GTX, and NEO. (A)Fluorescence quenching response of STX and its analogs to MIP-QDs and NIP-QDs; (B) The imprinting factors of MIP-QDs by STX and its analogs; MIP-QDs, 15.0 mg/L; STX concentration, 60.0 μg/L.

3.5. Application of MIP-QDs on the STX detection in shellfish samples

Under optimal conditions, the fabricated fluorescence nanosensor based on the MIP-QDs was successfully applied for STX detection. The fluorescence quenching response in the developed system followed the Stern-Volmer equation. As shown in Fig. 9, the fluorescence intensity of the MIP-QDs decreased when the template concentrations sequentially increased. The Stern-Volmer plots of the MIP-QDs exhibited excellent linearity in the range of 20.0–100.0 μg/L with a correlation coefficient of 0.9988.

The practicality of fluorescence nanosensor based on MIP-QDs as optosensing materials for highly selective and sensitive STX detection in shellfish samples was further explored. A recovery study was conducted, and the results were illustrated in Table. 1. After the samples were simply extracted and purified as the procedure of "*2.6. Sample preparation*", the mean recoveries ranged from 89.4% to 102.4%, and the intra-day and inter-day precision (RSD) were both less than 6.3%. Furthermore, the LOD, which was defined as the STX spiked concentration that quenches the standard deviation of the blank shellfish samples by threefold, was 0.3 μg/kg.

Moreover, the analytical performance of the developed nanosensor based on the MIP-QDs was compared with previously reported works for the determination of STX and summarized in Table 2. The developed method provided the excellent accuracy (Recovery) and precision (RSD), which were comparable or better than those of other reported methods. In addition, the sensitiv-

Table 1
Analysis of STX in spiked shellfish samples using the fluorescence nanosensor based on MIP-QDs; n = 3.

PST	Types	Spiked level (μg/kg)	Intra-day(%)		Inter-day(%)	
			Recovery	RSD	Recovery	RSD
STX	*Mytilus edulis*	30.0	97.4	3.2	101.2	3.9
		40.0	89.4	4.2	99.2	3.9
		50.0	102.4	4.6	102.1	4.5
	Oyster	30.0	100.2	5.7	101.0	6.0
		40.0	98.8	4.3	89.8	5.2
		50.0	89.6	5.6	98.3	6.3
	Meretrix meretrix	30.0	98.6	4.7	99.8	5.9
		40.0	92.9	5.7	101.5	5.4
		50.0	98.6	4.4	96.4	5.6

Table 2
The performance comparison of proposed method with other methods.

Method	Linear range (μg/kg)	RSD(%)	LOD (μg/kg)	Recovery (%)	Refs.
Fluorescence nanosensor	20.0–100.0	6.3	0.3	89.4–102.4	This work
CEIA-EC	0.8–66.6	6.5	4.3	92.5–107.6	[32]
CE-ICP-MS	15.0–179.4	7.0	1.1	93.0–110.0	[33]
HILIC-MS/MS	8.1–225.5	15.8	2.9	71.3–104.6	[34]
Competitive biosensor	10.0–2000.0	6.5	0.5	101.4–107.3	[35]

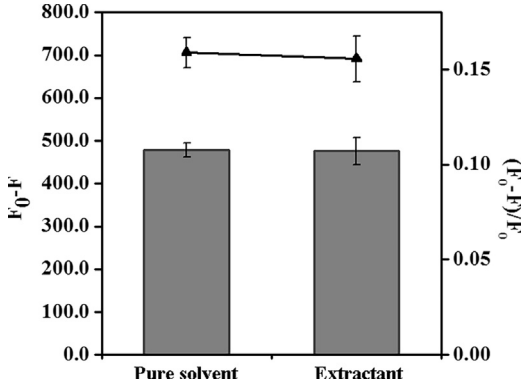

Fig. 8. Fluorescence quenching (the bars) and quenching efficiency (the triangles) of STX on MIP-QDs under pure solvent and sample extractant. MIP-QDs, 15.0 mg/L; STX concentration, 60.0 μg/L.

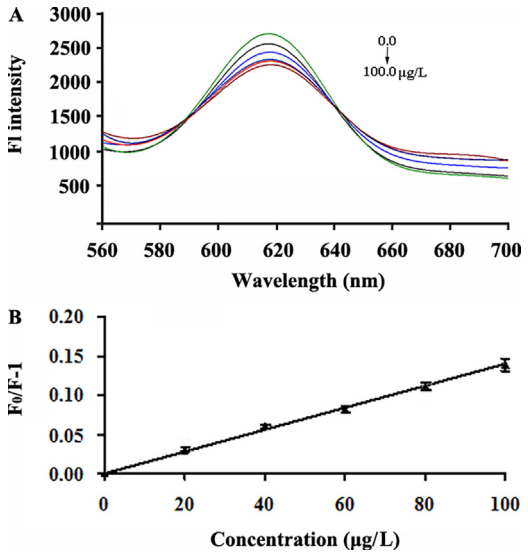

Fig. 9. Fluorescence emission spectra of MIP-QDs added with increasing quantities of STX (A) and Stern-Volmer plot (B). MIP-QDs, 15.0 mg/L; STX concentration, 20.0-100.0 μg/L.

ity of this method was improved due to the high selectivity of MIPs. Furthermore, compared with chromatographic method, the fluorescence nanosensor is simpler, lower time and solvent consumption, and easier operation.

4. Conclusions

We developed a novel fluorescence nanosensor approach for the detection of STX in shellfish. The method is based on MIP-QDs that were synthesized and characterized for the first time in this study. The morphology observation and FT-IR spectra of the synthesized MIP-QDs indicated that the MIP layer was successfully anchored onto the QDs. Furthermore, the fluorescence of the artificial MIP-QDs was more strongly quenched by the STX compared with NIP-QDs, indicating that the MIP-QDs can specifically recognize the corresponding template molecule. Under optimal conditions, the MIP-QDs showed good selectivity for STX versus its analogs, and the developed fluorescence nanosensor based on MIP-QDs had an excellent linear range, low LOD, good accuracy and precision for detecting STX in shellfish samples. The performance of the developed fluorescence nanosensor shows high potential for quick screening and accurate analysis of STX residue in monitoring programs.

Acknowledgements

This work was supported by the National Natural Science Foundation of China (No. 31372572), the Zhejiang Provincial Natural Science Foundation of China (LR16C190001), the Public Science and Technology Research Funds Projects of Ocean (No. 201305010), the Technology Innovation Team of Ningbo city (2015C110018), the project of Zhejiang Provincial Food and Drug Administration (2015002), Supported by the Open Fund of Zhejiang Provincial Top Key Discipline of Aquaculture in Ningbo University (xkzsc1515), and the K.C. Wong Magna Fund in Ningbo University.

References

[1] B. Christian, B. Luckas, Determination of marine biotoxins relevant for regulations: from the mouse bioassay to coupled LC–MS methods, Anal. Bioanal. Chem. 391 (2008) 117–134.
[2] M. Wiese, P.M. D'agostino, T.K. Mihali, M.C. Moffitt, B.A. Neilan, Neurotoxic alkaloids: saxitoxin and its analogs, Mar. Drugs 8 (2010) 2185–2211.

[3] G.S. Wiberg, N.R. Stephenson, Toxicologic studies on paralytic shellfish poison, Toxicol. Appl. Pharm. 2 (1960) 607–615.
[4] J. Machado, J. Azevedo, V. Vasconcelos, A. Campos, Mode of action and toxicity of major cyanobacterial toxins and corresponding chemical variants microbial, Toxins (2016) 1–24.
[5] L.M. Durán-Riveroll, A.D. Cembella, C.J. Band-Schmidt, J.J. Bustillos-Guzmán, J. Correa-Basurto, Toxins 8 (2016) 129.
[6] A.L. Bogomolni, A.L. Bass, S. Fire, L. Jasperse, M. Levin, O. Nielsen, G. Waring, S.D. Guise, Saxitoxin increases phocine distemper virus replication upon in-vitro infection in harbor seal immune cells, Harmful Algae 51 (2016) 89–96.
[7] T.A. Gill, J.W. Thompson, S. Gould, Thermal resistance of paralytic shellfish poison in soft-shell clams, J. Food. Protect. 48 (1985) 659–662.
[8] A. Alfonso, M.C. Louzao, M.R. Vieytes, L.M. Botana, Comparative study of the stability of saxitoxin and neosaxitoxin in acidic solutions and lyophilized samples, Toxicon 32 (1994) 1593–1598.
[9] L.M. Rangel, K.A. Ger, L.H. Silva, M.C.S. Soares, E.J. Faassen, M. Lürling, Toxicity overrides morphology on Cylindrospermopsis raciborskii grazing resistance to the calanoid copepod Eudiaptomus gracilis, Microb. Ecol 71 (2016) 835–844.
[10] J.C. Wekell, J. Hurst, K.A. Lefebvre, The origin of the regulatory limits for PSP and ASP toxins in shellfish, J. Shellfish Res. 23 (2004) 927–930.
[11] P. Truman, R.J. Lake, Comparison of mouse bioassay and sodium channel cytotoxicity assay for detecting paralytic shellfish poisoning toxins in shellfish extracts, J. AOAC Int. 79 (1995) 1130–1133.
[12] H. Suzuki, K. Machii, Comparison of toxicity between saxitoxin and decarbamoyl saxitoxin in the mouse bioassay for paralytic shellfish poisoning toxins, J. Vet. Med. Sci. 76 (2014) 1523–1525.
[13] L. Zou, C. Wu, Q. Wang, J. Zhou, K. Su, H. Li, N. Hu, P. Wang, An improved sensitive assay for the detection of PSP toxins with neuroblastoma cell-based impedance biosensor, Biosens. Bioelectron. 67 (2015) 458–464.
[14] R. Watanabe, R. Matsushima, T. Harada, H. Oikawa, M. Murata, T. Suzuki, Quantitative determination of paralytic shellfish toxins in cultured toxic algae by LC-MS/MS, Food. Addit. Contam. 30 (2013) 1351–1357.
[15] R.E. Gawley, H. Mao, M.M. Haque, J.B. Thorne, J.S. Pharr, Visible fluorescence chemosensor for saxitoxin, J. Org. Chem. 72 (2007) 2187–2191.
[16] S. Gao, X. Zheng, B. Hu, M. Sun, J. Wu, B. Jiao, L. Wang, Enzyme-linked, aptamer-based, competitive biolayer interferometry biosensor for palytoxin, Biosens. Bioelectron. 89 (2017) 952–958.
[17] L. Hou, L. Jiang, Y. Song, Y. Ding, J. Zhang, X. Wu, D. Tang, Amperometric aptasensor for saxitoxin using a gold electrode modified with carbon nanotubes on a self-assembled monolayer, and methylene blue as an electrochemical indicator probe, Microchim. Acta. 183 (2016) 1971–1980.
[18] T. Yamasaki, S. Miyake, S. Nakano, H. Morimura, Y. Hirakawa, M. Nagao, Y. Iijima, H. Narita, S. Ichiyama, Development of a surface plasmon resonance-based immunosensor for detection of 10 major o-antigens on shiga toxin-producing escherichia coli, with a gel displacement technique to remove bound bacteria, Anal. Chem. 88 (2016) 6711–6717.
[19] K. Campbell, A.C. Huet, C. Charlier, C. Higgins, P. Delahaut, C.T. Elliott, Comparison of ELISA and SPR biosensor technology for the detection of paralytic shellfish poisoning toxins, J. Chromatogr. B 877 (2009) 4079–4089.
[20] V. Scognamiglio, A. Antonacci, M.D. Lambreva, S.C. Litescu, G. Rea, Synthetic biology and biomimetic chemistry as converging technologies fostering a new generation of smart biosensors, Biosens. Bioelectron. 74 (2015) 1076–1086.
[21] Y. Li, T. Wen, C. Xue, Q. Han, Y. Wang, J. Hong, X. Zhou, H. Jiang, RGO LBL modified biomimetic electrochemical sensor for detection of Sildenafil in herbal sexual healthproducts, Biosens. Bioelectron. 42 (2013) 287–292.
[22] M. Stanisavljevic, S. Krizkova, M. Vaculovicova, R. Kizek, V. Adam, Quantum dots-fluorescence resonance energy transfer-based nanosensors and their application, Biosens. Bioelectron. 74 (2015) 562–574.
[23] M. Mehrzad-Samarin, F. Faridbod, A.S. Dezfuli, M.R. Ganjali, A novel metronidazole fluorescent nanosensor based on graphene quantum dots embedded silica molecularly imprinted polymer, Biosens. Bioelectron. 92 (2017) 618–623.
[24] B.B. Prasad, D. Jauhari, A dual-template biomimetic molecularly imprinted dendrimer-based piezoelectric sensor for ultratrace analysis of organochlorine pesticides, Sens. Actuatuators B-Chem. 207 (2015) 542–551.
[25] R.B. Queirós, A. Guedes, P. Marques, J. Noronha, M.G.F. Sales, Recycling old screen-printed electrodes with newly designed plastic antibodies on the wall of carbon nanotubes as sensory element for in situ detection of bacterial toxins in water, Sens. Actuators. B-Chem. 189 (2013) 21–29.
[26] K. Matsumoto, B.D.B. Tiu, A. Kawamura, R.C. Advincula, T. Miyata, QCM sensing of bisphenol A using molecularly imprinted hydrogel/conducting polymer matrix, Polym. J. 48 (2016) 525–532.
[27] H. Ding, H.F. Jiao, X.Z. Shi, A.L. Sun, X.Q. Guo, D.X. Li, J. Chen, Molecularly imprinted optosensing sensor for highly selective and sensitive recognition of sulfadiazine in seawater and shrimp samples, Sens. Actuators. B-Chem. 246 (2017) 510–517.
[28] M. Stobiecka, Novel plasmonic field-enhanced nanoassay for trace detection of proteins, Biosens. Bioelectron. 55 (2014) 379–385.
[29] H. Li, Y. Li, J. Cheng, Molecularly imprinted silica nanospheres embedded CdSe quantum dots for highly selective and sensitive optosensing of pyrethroids, Chem. Mater. 22 (2010) 2451–2457.
[30] L.E. Llewellyn, Saxitoxin, a toxic marine natural product that targets a multitude of receptors, Nat. Prod. Rep. 23 (2006) 200–222.
[31] S. Xu, H. Lu, J. Li, X. Song, A. Wang, L. Chen, S. Han, Dummy molecularly imprinted polymers-capped CdTe quantum dots for the fluorescent sensing of 2 4, 6-trinitrotoluene, ACS. Appl. Mater. Inter. 5 (2013) 8146–8154.
[32] X. Zhang, Z. Zhang, Capillary electrophoresis-based immunoassay with electrochemical detection as rapid method for determination of saxitoxin and decarbamoylsaxitoxin in shellfish samples, J. Food Compos. Anal. 28 (2012) 61–68.
[33] Y. He, F. Mo, D. Chen, L. Xu, Y. Wu, F. Fu, Capillary electrophoresis inductively coupled plasma mass spectrometry combined with metal tag for ultrasensitively determining trace saxitoxin in seafood, Electrophoresis 38 (2017) 469–476.
[34] L.Y. Zhuo, Y.C. Yin, W.S. Fu, B. Qiu, Z.Y. Lin, Y.Q. Yang, L.M. Chen, R. vJ. Li, G.N. Chen, Determination of paralytic shellfish poisoning toxins by HILIC?MS/MS coupled with dispersive solid phase extraction, Food Chem. 137 (2013) 115–121.
[35] S.X. Gao, X. Zheng, J.H. Wu, A biolayer interferometry-based competitive biosensor for rapid and sensitive detection of saxitoxin, Sens. Actuators B 246 (2017) 169–174.

Biographies

Ai-Li Sun Female, Associate professor, Major: Aquaculture; E-mail: sunaili@nbu.edu.cn

Ji-Ye Chai Male, Master, Major: Food safety; E-mail: 1242668658@qq.com

Ting-Ting Xiao Female, Master, Major: Food safety; E-mail: 1245667383@qq.com

Xi-Zhi Shi Male, Professor, Major: Food safety; E-mail: shixizhi@nbu.edu.cn

Xun-Jia Li Male, Master, Major: Food safety; E-mail: 630585969@qq.com

Qiao-Ling Zhao Female, Master, Major: Food safety; E-mail: nbzx12@163.com

De-Xiang Li Male, Master, Major: Food safety; E-mail: 375204280@qq.com

Jiong Chen Male, Professor, Major: Aquaculture; E-mail: dhnb84@126.com; chenjiong@nbu.edu.cn